Direct observation of a local thermal vibration anomaly in a quasicrystal

Eiji Abe*†, S. J. Pennycook* & A. P. Tsai†

** Condensed Matter Sciences Division, Oak Ridge National Laboratory, Oak Ridge, Tennessee 37830, USA*
† National Institute for Materials Science and SORST, Japan Science and Technology Corporation, 1-2-1 Sengen, Tsukuba 305-0047, Japan

Quasicrystals have long-range order with symmetries that are incompatible with periodicity, and are often described with reference to a higher-dimensional analogue of a periodic lattice[1–3]. Within the context of this 'hyperspace' crystallography, lattice dynamics of quasicrystals can be described by a combination of lattice vibrations and atomic fluctuations—phonons and phasons[1,4]. However, it is difficult to see localized fluctuations in a real-space quasicrystal structure, and so the nature of phason-related fluctuations and their contribution to thermodynamic stability are still not fully understood. Here we use atomic-resolution annular dark-field scanning transmission electron microscopy to map directly the change in thermal diffuse scattering intensity distribution in the quasicrystal, through *in situ* high-temperature observation of decagonal $Al_{72}Ni_{20}Co_8$. We find that, at 1,100 K, a local anomaly of atomic vibrations becomes significant at specific atomic sites in the structure. The distribution of these localized vibrations is not random but well-correlated, with a quasiperiodic length scale of 2 nm. We are able to explain this feature by an anomalous temperature (Debye–Waller) factor for the Al atoms that sit at the phason-related sites defined within the framework of hyperspace crystallography. The present results therefore provide a direct observation of local thermal vibration anomalies in a solid.

Within the hyperspace n-dimensional ($n \geq 4$) crystallography, the quasiperiodic structure can be generated from the n-dimensional periodic lattice decorated by so-called occupation domains[3] (or atomic surfaces) that can be converted into the atomic arrangement of the real quasicrystal. The n-dimensional crystal is defined by n basis vectors—the number of vectors is more than the real dimensions so as to incorporate the quasicrystal symmetry, giving rise to a unique elastic degree of freedom specific to quasicrystals; this results in 'phasons', in addition to the usual phonons that are present in crystals. The phason has no counterpart in periodic crystals, and hence the Debye–Waller (DW) factor of a quasicrystal may have both phonon and phason contributions[1,5,6], written as;

$$M = M_{\text{phonon}} + M_{\text{phason}} \quad (1)$$

Here, M is the DW factor defined by mean-square thermal vibration amplitude, $\langle u^2 \rangle$, of the atoms. The occupation domains are generally not continuous in quasicrystals, and a phason model predicts a significant fluctuation that smears the surfaces (edges) of the occupation domains. This surface fluctuation causes a local anomaly of the DW factor at the corresponding real-space atomic sites, but does not destroy the long-range quasiperiodic order; it causes a reduction in the Bragg intensity, and consequently some additional diffuse scattering.

The existence of phason-related atomic fluctuations is a critical factor in the thermodynamic stability of quasicrystals, whatever their origin; the context could be a random-tiling-like realization[7] where phason fluctuations are essential to provide entropic stabilization, or an unlocked state[8] of an intrinsically energy-minimized perfect quasicrystal. In both cases, phason fluctuations are expected to be significant above some critical temperature. So far, numerous experimental measurements of DW factors[9,10], phason atomic jumps[11,12], large-scale (~2 nm) phason tile-flips[13] and phason-related structural defects[14,15] have been attempted by various techniques. However, there has been no direct evidence on where such localized atomic fluctuations take place in the real-space quasicrystal structure.

Annular dark-field scanning transmission electron microscopy (ADF-STEM) provides atomic-resolution images by effectively illuminating each atomic column one-by-one as a finely focused probe is scanned across a thin crystalline specimen. The annular detector generates an intensity map of the scattered electrons with atomic-number (Z) contrast[16]. Because the detector is at a high angle, the scattering is dominated by phonon scattering events (that is, thermal diffuse scattering, TDS), and is therefore very sensitive to the DW factor; an Einstein model of independently vibrating atoms is valid for describing the multiphonon contribution that dominates high-angle diffuse scattering. Thus, the TDS cross-section (σ_{TDS}) over the range of the annular detector is given by[16]:

$$f'_{\text{HA}}(M,s) \approx \sigma_{\text{TDS}} \propto \int_{\text{detector}} f^2(s)[1 - \exp(-2Ms^2)]\,\mathrm{d}^2\mathrm{s} \quad (2)$$

where $f'_{\text{HA}}(M,s)$ is the absorptive atomic form factor for high-angle scatterings, $f(s)$ is the atomic form factor for elastic scatterings (with $s = \theta/2\lambda$, where θ is the scattering angle and λ is the electron wavelength) and M is the DW factor. The thermal vibration is responsible for destroying the coherence along the beam direction, and hence the scattering is assumed to be generated incoherently from individual atoms. Thus, to a good approximation, the intensity of each illuminated atomic column will be directly dependent on the σ_{TDS} within the relevant column (although TDS described by σ_{TDS} does not reflect any fine details[17] of the high-angle diffraction pattern, it is sufficient for estimating the integrated intensity reaching the detector).

Here we present the direct observation of local anomalies of the DW factor in a quasicrystal, through an *in situ* high-temperature ADF-STEM observation of decagonal $Al_{72}Ni_{20}Co_8$ for which a nearly perfect, ideal quasiperiodic structure (referred to as a basic AlNiCo structure) can be obtained by annealing at 1,100 K (the thermodynamically stable phase)[18]. Because the decagonal structure has a two-dimensional character described as a periodic stacking of quasiperiodic planes, ADF-STEM with the incident beam along a ten-fold symmetry axis enables us to observe directly the quasiperiodic arrangement of atoms[19,20]. In the observation at room temperature (300 K) of the water-quenched sample after annealing at 1,100 K (Fig.1a), the ADF-STEM image highlights the transition metal (TM: Ni or Co) positions relative to the Al, owing to the $f^2(s)$

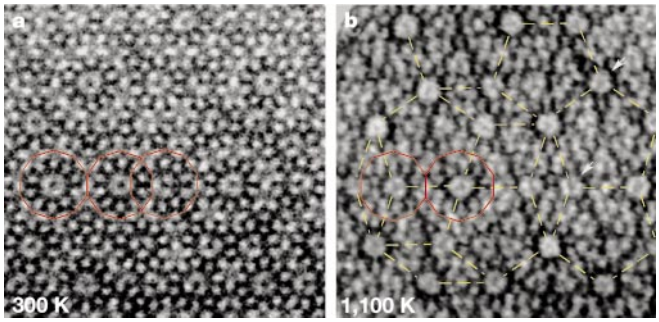

Figure 1 Atomic-resolution annular dark-field scanning transmission electron microscope (ADF-STEM) images of decagonal $Al_{72}Ni_{20}Co_8$. These were taken at **a**, 300 K and **b**, 1,100 K, by collecting the electrons scattered at angles between approximately 45 and 100 mrad ($0.9 \leq s \leq 2.0$) with a 200-kV STEM. The images were obtained, although not from exactly the same region, from the near-edge regions of the same cleavage grain, so that the specimen thickness is comparable. Therefore, contrast differences between **a** and **b** are due to the different temperature, not to changes in specimen thickness. By connecting the centre of 2-nm decagonal clusters (red) that reveal significant temperature-dependent contrast change, pentagonal quasiperiodic tiling (yellow) with an edge length of 2 nm can be drawn in **b**.

dependence of the contrast (equation (2)). Tracing the major brightest spots provided an excellent match to a perfect quasi-periodic pattern described by overlapping decagonal tiles[21] (Gummelt tiling[22]) with a diameter of 2 nm, some of which are outlined in Fig.1a, leading to a quasi-unit-cell model structure based on the atomic cluster with broken ten-fold symmetry[21,23,24]. But when the sample is heated and held at a temperature of approximately 1,100 K in the microscope, we find a remarkable change in the relative contrast (compare Fig. 1b with Fig. 1a). It is evident that a significant enhancement in contrast appears at some specified places that can be well represented by the pentagonal Penrose tiling with an edge length of 2 nm, although a local matching rule seems to be not completely maintained (note that pentagonal Penrose tiling is uniquely related to Gummelt's tiling by connecting the specified decagons separated by 2 nm).

Further, we notice that anomalous contrast occurs at cores of the decagons (Fig. 1b); a representative feature is shown in Fig. 2b and d. (A few other clusters reveal complicated contrasts at the core, including five-fold symmetry-like appearance of the bright spots indicated by arrows in Fig. 1b, although these clusters are rare compared to the clusters shown in Fig. 2. Possible interpretations of this issue will be discussed later.) Viewing carefully the interior contrast of the decagon in Fig. 2b and d, an increase of intensity is found to be significant at the positions indicated by arrowheads, which are the Al sites in the decagonal cluster model[23] (Fig. 2e). The intensity profiles show that the Al atom at the core, denoted as Alα, in fact shows stronger contrast at 1,100 K than that at 300 K. We confirmed that this temperature-dependent contrast change is reversible; that is, after cooling down to 300 K from 1,100 K, the anomalous contrast regions become darker again. It should be noted that the intensity at the Alα site ($I_{Al\alpha}$) is originally stronger than that of the other Al sites at 300 K (Fig. 2b); the $I_{Al\alpha}$ is found to vary significantly depending on the angular range of the detector (Fig. 2a–c), whereas the intensities of the other Al and TM atoms do not—I_{TM}/I_{Al} is almost constant at any angle-range. These angle-dependent as well as temperature-dependent (reversible) anomalous contrasts can naturally be attributed to a local anomaly of the DW factor, as expected through equation (2); assuming that the DW factor effect is equivalent for all the Al sites, neither of these dependences is expected.

We now interpret the significant increase of $I_{Al\alpha}$ in terms of atomic vibration amplitudes, $\langle u^2 \rangle$, for the observations both at 300 K and 1,100 K; we assume that there is no static column distortion effect[16] contributing to the anomalous $I_{Al\alpha}$ even at 300 K. (Static transverse displacements of the Alα atoms cause relaxations of the nearest-neighbour TM atoms; these TM atoms are also distorted, and are expected to reveal anomalous contrast compared to the other TM atoms; however, they do not show any significant angle-dependent contrast change—I_{TM}/I_{Al} is almost constant in Fig. 2a–c.) Note that I_{TM}/I_{Al} does not change much, even after increasing the temperature (Fig. 2d), indicating that the effects of temperature on the DW factors of these Al and TM atoms

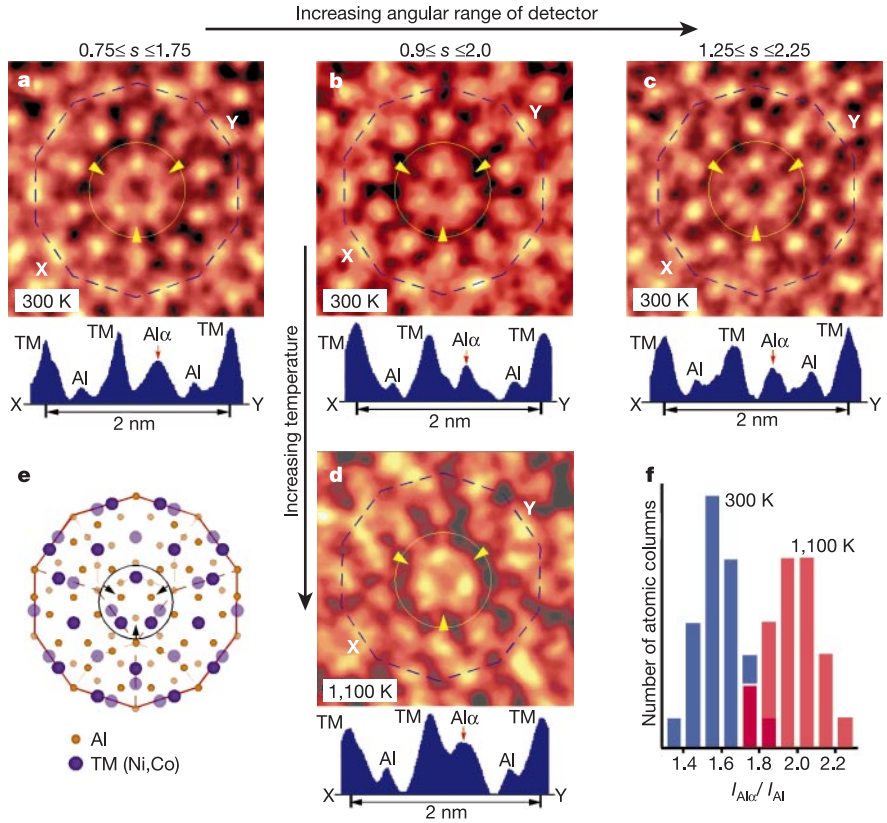

Figure 2 A decagonal cluster with a diameter of about 2 nm, a structural unit of $Al_{72}Ni_{20}Co_8$. The clusters were observed at 300 K (**a**–**c**) with different angular ranges of the detector, and at 1,100 K (**d**); also shown are the corresponding line profiles across *X*–*Y*. Images of **a** and **c** are obtained from the same cluster, using the 300-kV STEM with detector angle ranges of about 30–70 mrad ($0.75 \leq s \leq 1.75$) and 50–90 mrad ($1.25 \leq s \leq 2.25$), respectively. Images **b** and **d** are enlargements of a part of Fig. 1a and b, respectively. The images **a**–**d** show significant contrast changes at the core of the cluster, particularly at the positions indicated by arrows, which correspond to the Alα sites denoted in the line profiles. **e**, Structural model of $Al_{72}Ni_{20}Co_8$ with a practical averaged configuration derived by superimposing all possible atomic positions in the quasi-unit-cell model (assuming perfect quasiperiodic atomic order, there appeared to be three variations of atomic arrangements in the interior of the cluster[23]). Structural refinements[27,28] based on single-crystal X-ray data converge on a nearly identical arrangement to this averaged configuration. The structure has two distinct atomic layers stacked along the periodic *c* axis; bold and pale dots denote the atoms at layers $c = 0$ and $c = 1/2$, respectively. **f**, Histograms of intensity ratios between the Alα and Al atomic columns, $I_{Al\alpha}/I_{Al}$, from the 200-kV STEM images at 300 K and 1,100 K. The column intensities were measured for about 30 decagonal clusters, revealing similar behaviour to that seen in **b** and **d**; these features are typical of the clusters located at the 2-nm-scale pentagonal Penrose lattice.

are almost equivalent, and small compared with that of the Alα. Thus, we normalize the $I_{Al\alpha}$ with reference to the I_{Al} at each temperature. In Fig. 2f we show histograms of $I_{Al\alpha}/I_{Al}$ distributions, in which the $I_{Al\alpha}/I_{Al}$ peaks at around ~1.5 and ~2.0 (assuming a gaussian distribution) for the observations at 300 K and 1,100 K, respectively. Both the temperature and angle dependences are fairly well explained by the σ_{TDS} for different $\langle u^2\rangle$ values; see the $\sigma^{Al}_{TDS} - \langle u^2\rangle$ curves calculated on the basis of equation (2) (Fig. 3).

With the angle range of $0.9 \leq s \leq 2.0$, the ratio of σ^{Al}_{TDS} between the standard Al (denoted as Als whose DW factor is assumed not to be temperature dependent) and the Alα, $\sigma^{Al\alpha}_{TDS}/\sigma^{Al}_{TDS}$, can be approximately 1.5 and 2.0 with the appropriate $\langle u^2\rangle$ values at each temperature, for example, $\sim 0.4 \times 10^{-4}$ nm^2 (Als), $\sim 0.9 \times 10^{-4}$ nm^2 (Alα at 300 K) and $> \sim 3.0 \times 10^{-4}$ nm^2 (Alα at 1,100 K); this reproduces well the observed temperature-dependent change of $I_{Al\alpha}/I_{Al}$ (note that these $\langle u^2\rangle$ values are only tentative and may be improved when a more accurate $f'_{HA}(M,s)$ is available). A systematic angle-dependent change of $I_{Al\alpha}/I_{Al}$ observed at 300 K is also explained well by these $\langle u^2\rangle$ differences; the Alα can reveal stronger contrast, relative to that of the Als, for the lower angle ranges (see red arrows in Fig. 3). Although the $\langle u^2\rangle$ at 1,100 K cannot be determined because σ_{TDS} saturates at large $\langle u^2\rangle$ values, we nevertheless emphasize that the observed anomalous contrast at the Alα site has been clearly correlated with differences in $\langle u^2\rangle$. This is, to our knowledge, the first direct observation of a local vibration anomaly in a solid.

Significantly large $\langle u^2\rangle$ at high temperature is consistent with the recent X-ray diffuse scattering measurements on the same sample of $Al_{72}Ni_{20}Co_8$, in which the overall $\langle u^2\rangle$ is suggested to be of the order of $\sim 1.0 \times 10^{-3}$ nm^2 (at 1,100 K) when compared with a uniform harmonic vibration[25]. The local anomalies of $\langle u^2\rangle$ in the present work imply significant anharmonicity at the Alα site. Similar anomalies might therefore be anticipated at the neighbouring TM sites, and some evidence of this is seen at 1,100 K (Fig. 2d). Further supporting evidence comes from recent molecular-dynamics simulations[26] of the structure at 1,000 K, which predicted the occurrence of DW factor anomalies for the Al atoms at the core of the 2-nm decagonal cluster.

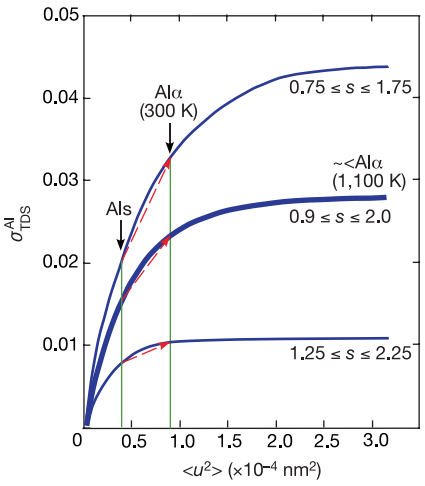

Figure 3 Estimates of the thermal diffuse scattering cross-section of Al (σ^{Al}_{TDS}; equation (2)) as a function of mean-square thermal vibration amplitude ($\langle u^2\rangle$). Data are shown for several detector angle (s) ranges (blue curves), and were calculated using the atomic form factor, $f(s)$, in ref. 30, by assuming an isotropic Debye–Waller (DW) factor ($M = 8\pi^2\langle u^2\rangle$). The bold curve ($0.9 \leq s \leq 2.0$) explains the temperature-dependent contrast change by assuming the appropriate $\langle u^2\rangle$ values for the Als (green line), Alα at 300 K (green line) and Alα at 1,100 K ($> \sim 3.0 \times 10^{-4}$ nm^2). Angle-dependent changes (at 300 K) expected from these $\langle u^2\rangle$ values are indicated by red arrows. Details are described in the text.

The Alα atoms, located at the centre of the decagonal clusters that are on the 2-nm-scale pentagonal quasiperiodic lattice vertices, are generated from the edge of the occupation domains (α in Fig. 4) within the hyperspace crystallographic description[27]. Thus, the present local DW factor anomaly can be attributed to significant fluctuations of the occupation domains in specified surface regions, which, in turn, indicate an occurrence of phasonic fluctuations—a perturbation of quasiperiodic order that can be described through M_{phason} (equation (1))—realized for the Alα atoms at the centre of the 2-nm cluster. Some Al atoms within the 2-nm cluster are also placed in a similar local environment to that of the Alα atoms—see the 'kite'[23] tiles drawn in Fig. 2e. However, they are symmetrically (crystallographically) not equivalent to the Alα site, and hence may not reveal any significant anomalies (that is, the atomic configuration in the kite tiles can be different[23] depending on their local-neighbour environment). An occurrence of DW factor anomalies at the Alα site is probably induced by the presence of the phason-flip atomic sites, denoted as β in Fig. 4, which are separated by less than a typical interatomic distance. Therefore the α and β sites cannot be occupied simultaneously, and the β sites, considered to be energetically similar to the Alα site[26], could act as vacancies in providing an effective space for relaxation; it is reasonable to assume that this causes significant anisotropy in the DW factor (Fig. 4). Although the resolution of the present STEM (~1.5 Å) is not sufficient to reveal this anisotropic behaviour, molecular-dynamics structural simulations[26] at 1,000 K have indicated an anisotropic DW factor

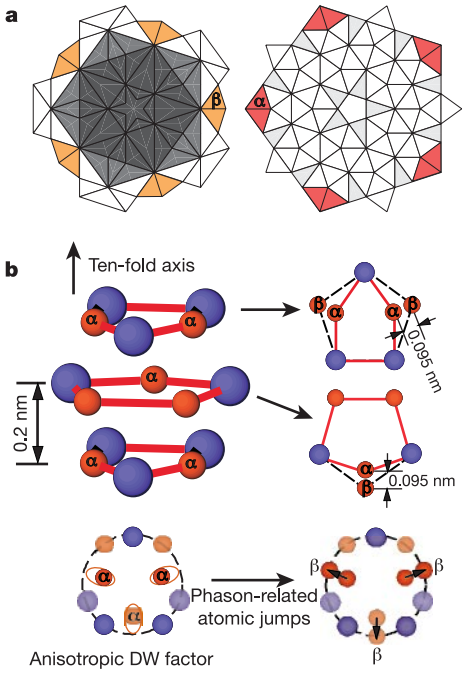

Figure 4 'Phason'-related atomic sites in the $Al_{72}Ni_{20}Co_8$ quasicrystal. **a**, Higher-dimensional, or 'hyperspace', crystallographic description of the decagonal $Al_{72}Ni_{20}Co_8$ structure[27]. Occupation domains are placed at (1/5, 1/5, 1/5, 1/5, 1/4) (left) and (2/5, 2/5, 2/5, 2/5, 1/4) (right) in the five-dimensional decagonal lattice with successful partitions assigned by Al and TM (transition metal), where the grey level represents the concentration of the TM atoms at relevant sites (see ref. 27 for details). Extra β portions (yellow) have been added to the edges of the occupation domain to generate phason-flip atomic sites with respect to the α sites that are generated from the α portions (red). **b**, Pentagonal columnar atomic configuration around the centre of the 2-nm decagonal cluster; orange and purple atoms represent Al and TM, respectively. Phason-related α and β sites are on the quasiperiodic atomic plane, separated by approximately 0.095 nm. Possible anisotropy of the DW factor of the Al atoms at the α sites and occurrence of atomic jumps into the β sites are described in the projected atomic positions shown below, where the pale atoms represent those at different levels along the ten-fold axis.

identical to that shown in Fig. 4.

Regarding diffusional atomic jumps at high temperature, it is natural to consider that the local vibration anomalies enhance the short-range diffusion of atoms located around the cluster centre with a help of a phason-site-mediated transport mechanism, causing occasional diffusion jumps of not only Al but also TM atoms into the phason β site. This explains a random occurrence of five-fold symmetry-like clusters at some places (Fig. 1b). Note that the atoms delivered to the β site by diffusion jump can be quenched in, so that they will be recognized as 'quenched phason-defects' (including chemical and site-occupation disorders that are significant at the core of the 2-nm clusters), which have in fact been detected by experimental measurements on the quenched sample[20,27,28].

Alternatively, five-fold-symmetric 2-nm clusters emerge as the thermodynamically stable configuration when the present high-temperature $Al_{72}Ni_{20}Co_8$ undergoes phase transition at lower temperatures ($\lesssim 990$ K, to a less-quasiperiodic ordered phase); this suggests that the phason β sites, metastable at high temperature, provide stable positions for TM atoms at low temperature. This also indicates that the above structural transition is closely related to phason-related atomic behaviour, which is significant at the centre of the 2-nm clusters, as shown in the present direct observation. □

Methods

Atomic-resolution images were taken by 200-kV (JEOL 2010F) and 300-kV (VG Microscopes, HB603U) scanning transmission electron microscopes, providing a minimum probe of approximately 0.150 nm and 0.126 nm, respectively. The former microscope was used for a high-temperature *in situ* observation. Specimens were prepared by crushing the bulk material and depositing it onto perforated amorphous carbon film supported on Cu grids; by this method, the surface amorphous layer, roughness, and contamination that are frequently induced by ion-milling and which strongly affect image contrast, can be avoided. Thus, the intensities measured from the present images give reliable information. Heating to 1,100 K in the microscope was achieved within 5 min, which effectively suppresses a phase transition that would occur at $\lesssim 990$ K during heating. The electron diffraction pattern taken at 1,100 K from the grain used for imaging (Fig. 1) confirmed that $Al_{72}Ni_{20}Co_8$ retains its basic AlNiCo structure during *in situ* high-temperature observation. Energy-dispersive X-ray spectroscopy showed no detectable compositional change of the grain before and after the heat treatment in the microscope.

Received 20 September; accepted 25 November 2002; doi:10.1038/nature01337.

1. Bak, P. Phenomenological theory of icosahedral incommensurate ("quasiperiodic") order in Mn-Al alloys. *Phys. Rev. Lett.* **54,** 1517–1519 (1985).
2. Janssen, T. Crystallography of quasi-crystals. *Acta Crystallogr. A* **42,** 261–271 (1986).
3. Yamamoto, A. Crystallography of quasiperiodic crystals. *Acta Crystallogr. A* **52,** 509–560 (1996).
4. Socolar, T., Lubensky, T. & Steinhardt, P. J. Phonons, phasons, and dislocations in quasicrystals. *Phys. Rev. B* **34,** 3345–3360 (1986).
5. Jaric, M. V. & Nelson, D. R. Diffuse scattering from quasicrystals. *Phys. Rev. B* **37,** 4458–4472 (1988).
6. Ishii, Y. Phason softening and structural transitions in icosahedral quasicrystals. *Phys. Rev. B* **45,** 5228–5239 (1992).
7. Henley, C. L. in *Quasicrystals: The State of the Art* (eds DiVincenzo, D. & Steinhardt, P. J.) 429–524 (World Scientific, Singapore, 1991).
8. Jeong, H. C. & Steinhardt, P. J. Finite-temperature elasticity phase transition in decagonal quasicrystals. *Phys. Rev. B* **48,** 9394–9403 (1993).
9. Bancel, P. A. in *Quasicrystals: The State of the Art* (eds DiVincenzo, D. & Steinhardt, P. J.) 17–55 (World Scientific, Singapore, 1991).
10. Colella, R., Zhang, Y., Sutter, J. P., Ehrlich, S. N. & Kycia, S. W. Debye-Waller factors in a quasicrystal. *Phys. Rev. B* **63,** 014202 (2000).
11. Dolinsek, J., Apih, T., Simsic, M. & Dubois, J. M. Self-diffusion in icosahedral $Al_{72.4}Pd_{20.5}Mn_{7.1}$ and phason percolation at low temperatures studied by ^{27}Al NMR. *Phys. Rev. Lett.* **82,** 572–575 (1999).
12. Coddens, G. & Steurer, W. Time-of–flight neutron-scattering study of phason hopping in decagonal Al-Co-Ni quasicrystals. *Phys. Rev. B* **60,** 270–276 (1999).
13. Edagawa, K., Suzuki, K. & Takeuchi, S. High resolution transmission electron microscopy observation of thermally fluctuating phasons in decagonal Al-Cu-Co. *Phys. Rev. Lett.* **85,** 1674–1677 (2000).
14. de Boissieu, M. *et al.* Diffuse scattering and phason elasticity in the AlPdMn icosahedral phase. *Phys. Rev. Lett.* **75,** 89–92 (1995).
15. Zeger, G., Plachke, D., Carstanjen, H. D. & Trebin, H.-R. Quasicrystalline d-AlCuCo identified as random tiling by ion channeling combined with particle-induced X-ray emission. *Phys. Rev. Lett.* **82,** 5273–5276 (1999).
16. Pennycook, S. J. & Jesson, D. E. High-resolution Z-contrast imaging of crystals. *Ultramicroscopy* **37,** 14–38 (1991); Atomic-resolution Z-contrast imaging of interfaces. *Acta Metall. Mater.* **40,** S149–S159 (1992).
17. Muller, D. A., Edward, B., Kirkland, E. J. & Silcox, J. Simulation of thermal diffuse scattering including a detailed phonon dispersion curve. *Ultramicroscopy* **86,** 371–380 (2001).
18. Ritsch, S. *et al.* Highly perfect decagonal Al-Co-Ni quasicrystal. *Phil. Mag. Lett.* **74,** 99–106 (1996).
19. Saitoh, K. *et al.* Structural study of an $Al_{72}Ni_{20}Co_8$ decagonal quasicrystal using the high-angle annular dark-field method. *Jpn. J. Appl. Phys.* **36,** L1400–L1402 (1997).
20. Yan, Y., Pennycook, S. J. & Tsai, A. P. Direct imaging of local chemical disorder and columnar vacancies in ideal decagonal Al-Ni-Co quasicrystals. *Phys. Rev. Lett.* **81,** 5145–5148 (1998).
21. Steinhardt, P. J. *et al.* Experimental verification of the quasi-unit-cell model of quasicrystal structure. *Nature* **396,** 55–57 (1998); correction *Nature* (**399**), 84 (1999).
22. Gummelt, P. Construction of Penrose tilings by a single aperiodic protoset. *Geom. Dedicata* **62,** 1–17 (1996).
23. Abe, E. *et al.* Quasi-unit cell model for an Al-Ni-Co ideal quasicrystal based on clusters with broken tenfold symmetry. *Phys. Rev. Lett.* **84,** 4609–4612 (2000).
24. Yan, Y. & Pennycook, S. J. Chemical ordering in $Al_{72}Ni_{20}Co_8$ decagonal quasicrystals. *Phys. Rev. Lett.* **86,** 1542–1545 (2001).
25. Abe, H. *et al.* Anomalous Debye-Waller factor associated with an order-disorder transformation in an $Al_{72}Ni_{20}Co_8$ decagonal quasicrystal. *J. Phys.* (submitted).
26. Henley, C. L., Mihalkovic, M. & Widom, M. Total-energy-based prediction for d(AlNiCo). *J. Alloys Comp.* **342,** 221–227 (2002).
27. Takakura, H., Yamamoto, A. & Tsai, A. P. The structure of decagonal $Al_{72}Ni_{20}Co_8$ quasicrystal. *Acta Crystallogr. A* **57,** 576–585 (2001).
28. Cervellino, A., Haibach, T. & Steurer, W. Structure solution of the basic decagonal Al-Co-Ni phase by the atomic surfaces modeling method. *Acta Crystallogr. B* **58,** 8–33 (2002).
29. Hiraga, K., Ohsuna, T. & Nishimura, S. An ordered arrangement of atom columnar clusters in a pentagonal quasiperiodic lattice of an Al-Ni-Co decagonal quasicrystal. *Phil. Mag. Lett.* **80,** 653–659 (2000).
30. Weickenmeier, A. & Kohl, H. Computation of absorptive form factors for high-energy electron diffraction. *Acta Crystallogr. A* **47,** 590–597 (1991).

Acknowledgements We thank H. Takakura, T. J. Sato, N. Tanaka, K. Ishizuka, M. Widom and C. L. Henley for discussions.

Competing interests statement The authors declare that they have no competing financial interests.

Correspondence and requests for materials should be addressed to E.A. (e-mail: abe.eiji@nims.go.jp).

Photocontrolled reversible release of guest molecules from coumarin-modified mesoporous silica

Nawal Kishor Mal, Masahiro Fujiwara & Yuko Tanaka

Kansai Center, National Institute of Advanced Industrial Science and Technology (AIST-Kansai), Ikeda, Osaka 563-8577, Japan

Since the discovery[1] of MCM-41 more than ten years ago, many investigations have explored the suitability of hexagonal mesoporous silicas for potential practical applications[2–4]. These range from catalysis[5,6] and optically active materials[7,8] to polymerization science[9–12], separation technology[3,13,14] and drug delivery[15–18], with recent successes in the fabrication of hybrid mesoporous organosilicas[19–21] expected to open up further application possibilities. Because the pore voids of this class of materials exhibit relatively narrow pore size distributions in the range of 2–4 nm in diameter, mesoporous silicas can selectively include organic compounds and release them continuously at a later stage. The functionalization of MCM-41 pore voids with photoactive derivatives[22–25] provides influence over the material's absorption behaviour, but full control over the release process remains difficult. Here we show that the uptake, storage and release of organic molecules in MCM-41 can be regulated through the photocontrolled and reversible intermolecular dimerization[26,27] of coumarin derivatives attached to the pore outlets. Successful functionalization requires uncalcined MCM-41 still filled with the template molecules that directed the formation of its pores, to ensure that coumarin derivatives attach preferentially to the pore outlets, rather than their inside walls. We find that this feature and the one-dimensional, isolated nature of the individual pores allow for efficient and reversible photocontrol over guest access to the material's interior.

